

Kramers-protected hardware-efficient error correction with Andreev spin qubits

Haoran Lu,¹ Isidora Araya Day,^{2,3} Anton R. Akhmerov,³ Bernard van Heck,⁴ and Valla Fatemi^{1,*}

¹*School of Applied and Engineering Physics, Cornell University, Ithaca, NY, 14853, USA*

²*QuTech, Delft University of Technology, Delft 2600 GA, The Netherlands*

³*Kavli Institute of Nanoscience, Delft University of Technology, 2600 GA Delft, The Netherlands*

⁴*Dipartimento di Fisica, Sapienza Università di Roma, Piazzale Aldo Moro 2, 00185 Rome, Italy*

(Dated: December 23, 2024)

We propose an architecture for bit flip error correction of Andreev spins that is protected by Kramers' degeneracy. Specifically, we show that a coupling network of linear inductors results in a static Hamiltonian composed of the stabilizers of a bit flip code. Thereby, without detuning from the Kramers' point, reflectometry off a single coupled resonator accomplishes a projective measurement of multiple stabilizers. We further use circuit-mediated spin couplings to design error correction operations and a complete set of logical quantum gates. The concept is experimentally feasible.

Andreev spin states are a new qubit platform composed of microscopic spin degrees of freedom that couple to macroscopic supercurrents [1–9]. Such direct integration of spins with superconductivity raises the prospect for strong or ultrastrong coupling to other superconducting degrees of freedom [10], including microwave-frequency plasmonic resonators and qubits [7–9, 11, 12] and to other Andreev spins [9]. One key consequence, as pointed out in a recent blueprint [13], is that Andreev spins can be the basis of a solid-state qubit platform with a ‘native’ ability to implement fast-tunable all-to-all connectivity. All-to-all connectivity brings significant potential advantages in overhead for both quantum error correction [14–17] and analog quantum simulation applications [18, 19].

Here, we show how Kramers' theorem [20] can gainfully constrain the connectivity, and with that we propose a hardware-efficient implementation of bit flip error detection that relies on a single readout resonator. Local spin control with multi-frequency drives and fast flux control further provide error correction and a complete set of logical gates. Experimentally demonstrated hardware is capable of accomplishing a demonstration of our proposal provided future improvements in spin dephasing times [6, 8]. In the main text we describe the salient aspects of our concept, and the appendices and published code provide technical details.

The Andreev spin can be modeled as a Josephson weak link with a spin-dependent energy-phase relation,

$$U_\sigma = E_0 \cos(\varphi) + E_\sigma \sigma_z \sin(\varphi), \quad (1)$$

where E_0 describes the spin-independent contribution (and may be positive or negative), $E_\sigma > 0$ describes the magnitude of the spin-dependent contribution, σ_z is the Pauli z matrix for the spin, and φ is the phase drop across the weak link. We remark that the orientation of σ_z is defined locally for each spin. Andreev spins can be concatenated in parallel or in series with each other and other inductive elements, such as linear inductors which have an energy-phase relation $U_L = \frac{\varphi_0^2}{2L} \varphi^2$, where $\varphi_0 = \hbar/2e$ is the reduced flux quantum.

For this work, we focus on a minimal circuit hosting three Andreev spins in series and linear inductors attached to each node, as shown in Fig. 1(a). Attachment of linear inductors to all nodes eliminates circuit offset charges which may contribute to setpoint drift [21]. The series configuration of spins is convenient for avoiding wiring crossovers and for controlling the range of interactions. Finally, the depicted field-effect gate electrodes serve two roles: tuning up the spins and accomplishing fast (down to ~ 20 ns), local spin control through electric dipole spin resonance (EDSR) [2, 7, 8, 22, 23]. We note that the basic physics described here is also compatible with parallel arrays and with non-linear inductive couplers [2, 9, 13].

For each spin configuration, the potential energy of the circuit needs to be minimized to obtain the ground state. Provided parasitic capacitances are all small enough, the dynamics of the internal degrees of freedom of the circuit are of sufficiently high frequency that they can be adiabatically eliminated [24]. An attached resonator with average frequency $\omega_{r,0}$ allows one dynamical phase degree of freedom across the entire array, which is used for readout. We implement an algorithm (detailed in the Appendix) to determine the energy and linear response of each spin configuration and their influence on the resonator.

For generic values of the circuit parameters, the eight distinct spin configurations have all different energies [2, 13] and an effective Hamiltonian of the circuit contains all possible Z-type couplings between any number of spins. If the magnetic fluxes in all loops are zero or π , a time-reversal symmetric configuration, Kramers' theorem guarantees that any coupling involving an odd number of spins vanishes [20]. The following static Hamiltonian results:

$$H_\sigma = J_{12}\sigma_{1,z}\sigma_{2,z} + J_{23}\sigma_{2,z}\sigma_{3,z} + J_{13}\sigma_{1,z}\sigma_{3,z}. \quad (2)$$

The specific values and signs of the spin-spin couplings J_{ij} depend on the details of the circuit and weak links, and so they are designable. We note in particular that this Hamiltonian form scales to more than three Andreev spin qubits (with the possible addition of higher order interactions involving even numbers of spins) and that the range

of the interaction depends on the vertical inductances.

We recognize the Hamiltonian (2) as being comprised of the stabilizers of a bit flip error correction code. The eigenstates are pairwise degenerate as guaranteed by Kramers' theorem, and the excited states are connected to the ground state by single spin flips as shown in Fig. 1(b). We remark that the Hamiltonian (2) was also described for parallel arrays [2, 13], but the physics of operation at Kramers' point as the idling point was not considered.

We now go further to consider the linear response to the phase drop across the array, which also respects the pairwise structure. We focus here on the inductance of the circuit that terminates a resonator, Fig. 1(a). The Andreev spin configuration affects the resonator frequency, resulting in contributions to the Hamiltonian at the Kramers point given by

$$H_r = \hbar\omega_{r,0}\hat{a}^\dagger\hat{a} + \sum_{i \neq j} \hbar\chi_{ij}\sigma_{i,z}\sigma_{j,z}\hat{a}^\dagger\hat{a}. \quad (3)$$

where \hat{a} is the lowering operator for the resonator, $\omega_{r,0}$ is

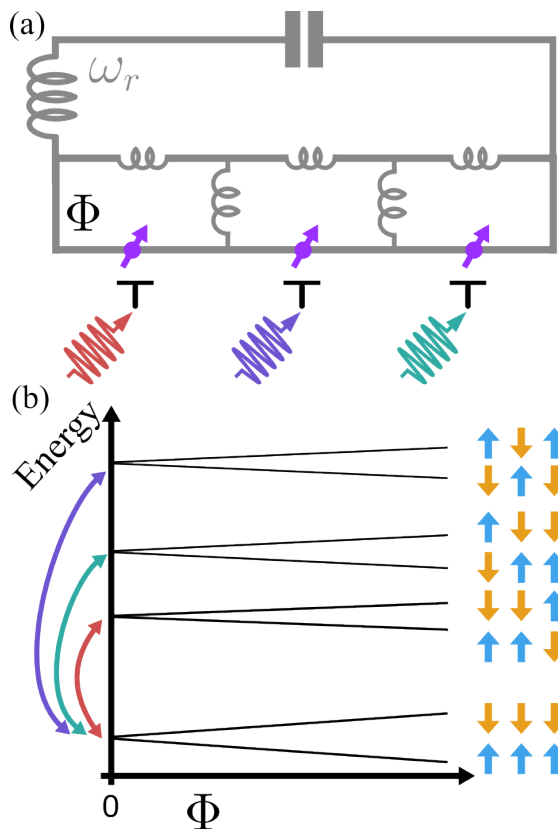


FIG. 1. (a) Circuit for minimal bit-flip encoding with Andreev spins. The field-effect gate lines on each spin (black) include DC gate voltages (not shown) and AC drive (colored). Control circuitry for flux Φ is not shown. (b) Schematic level structure as a function of flux, with the Kramers' point at zero flux. Colored arrows correspond to EDSR-induced single-spin transitions between the logical manifold (lowest) and the error manifolds while they remain degenerate.

the spin-unconditional resonator frequency, and χ_{ij} are spin-conditional frequency shifts. The total static Hamiltonian is then $H = H_\sigma + H_r$. Therefore, a microwave reflectometry measurement commonly used on Andreev spins and superconducting qubits [5, 22, 25–27] would accomplish projective measurement of the stabilizers, provided that the shifts χ_{ij} are different. We note that, as before, Kramers' theorem guarantees that only coupling terms between two spins appear in H_r . The absence of single-spin terms avoids the need to fine-tune the matching of resonator shifts due to individual qubits, as is the case with e.g. superconducting qubit architectures, in order to perform error detection [28–30].

This scheme also allows error correction without deviating from Kramers' point. The many-body spin configurations related by a *single* spin flip are not time-reversed partners: a local EDSR drive to spin j accomplishes $H_{d,j} \approx M_j\sigma_{j,x} \sum_{k \neq j} A_{kj}\sigma_{k,z}$, where M encloses a matrix element scale and drive amplitude, and A_{kj} are dimensionless weights proportional to spin-induced phase shifts; A_{kj} is nonzero because spin-spin interactions mediated by the inductors ensure that the equilibrium value of the phase difference across each individual junction is nonzero and depends on the spin configuration. This results in a nonzero matrix element to ESDR control (see Appendix for details). Therefore, the stabilizer readout may be followed by a single EDSR π pulse on the relevant spin to restore the system to the logical manifold. We remark that our scheme can extend beyond three spins to N spins for higher-order bit flip error correction.

We now describe available logical quantum gates, which are computationally complete. First, we address logical gates that mix or exchange the logical codewords. We note that each spin has two distinct spin-flip transition frequencies: one when the other two spins are aligned, and one where the other two spins are anti-aligned, per Fig. 2. Therefore, in order to locally drive a Rabi oscillation of a single spin in a way that is not selective of the configuration of the other spins, a two-frequency drive is needed. Such multi-frequency control has been implemented at RF frequencies in other solid-state qubit contexts [31–34].

With single spin control, the logical \bar{X} and \bar{Y} are transversal, accomplished by sequencing single spin π pulses, e.g. by EDSR: $\bar{X} = \sigma_{1,x}\sigma_{2,x}\sigma_{3,x}$. For the Hadamard \bar{H} gate, we propose the following protocol. We assume initialization in the logical manifold, $|\psi\rangle = a|\uparrow\uparrow\uparrow\rangle + b|\downarrow\downarrow\downarrow\rangle$. Then we implement the single-spin H gate on each spin to generate the state $|\psi\rangle = a|\rightarrow\rightarrow\rightarrow\rangle + b|\leftarrow\leftarrow\leftarrow\rangle$ (where $|\rightarrow\rangle$ and $|\leftarrow\rangle$ are the eigenstates of σ_x). A stabilizer measurement projects the state into one of the degenerate manifolds, with an \bar{H} gate applied to the logical manifold and an $\bar{X}\bar{H}$ gate applied to the other manifolds. If the logical manifold is not measured, performing error correction together with the logical \bar{X} finishes the \bar{H} gate.

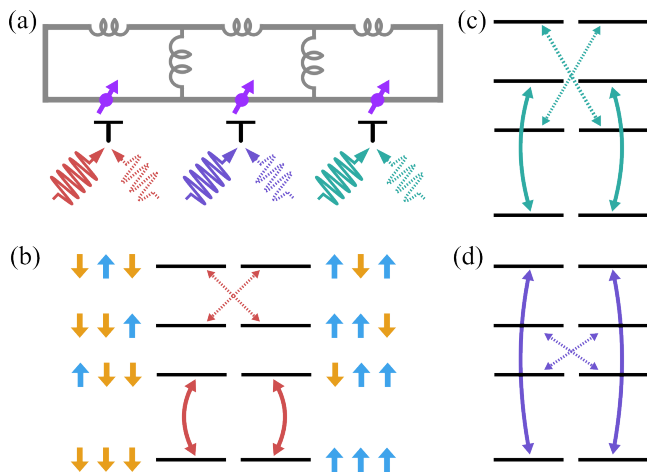


FIG. 2. Driving a single spin locally (a) can give unconditional spin flips at Kramers' point when two drive frequencies are used, as shown for the first (b), third (c), and second (d) spins.

Finally, a continuous logical phase gate $\bar{P}(\theta)$ can be accomplished by local flux control, completing the logical gate set. Consider the dispersion in flux shown in Figure 1(b). A local flux pulse $\Phi(t)$ detunes the energy difference ΔE between the many-body spin configurations within (and between) the computational manifolds. By ensuring that the flux starts and ends at zero, $\Phi(0) = \Phi(T) = 0$, the total accumulated logical phase difference θ is $\theta = \hbar^{-1} \int_0^T [E_{\uparrow\uparrow\uparrow}(\Phi(t)) - E_{\downarrow\downarrow\downarrow}(\Phi(t))] dt$. Crucially, $\bar{P}(\theta)$ includes non-Clifford gates, such as $\bar{T} = \bar{P}(\frac{\pi}{8})$, the logical \bar{T} gate. We note that this does come at the cost of breaking the protection afforded by Kramers' theorem while the gate is being applied.

The experimental feasibility of our concept requires balancing the energy scales of the Andreev spins (per Eq. (1)) and the characteristic energy scales of the inductors $\varphi_0^2/2L$. Typical measured values for E_J and E_σ range from 0.1 to 1 GHz [4–9, 22, 23]. We find that by using inductors of the scale 1 to 10 nH, which are commonly implemented [5, 23, 35, 36], we can achieve couplings $J_{ij}/2\pi$ at the MHz scale. This is sufficient for gates as fast as ~ 100 ns with baseband control. We note that the required inductance is inversely proportional to E_σ . Modeling the coupling to a typical distributed-element resonator from previous Andreev spin experiments [5, 23], the resonator frequency shifts $\chi_{ij}/2\pi$ are predicted to be 0.1 to 1 MHz, which is a standard range for single-shot dispersive readout in a similar duration. Finally, we estimate the EDSR-activating parameter $A_{kj} \gtrsim 0.01$, sufficient for gate driving. We note that by entering the non-perturbative circuit coupling regime in which the coupling inductances are comparable to the weak link inductance (such as proposed and recently accomplished in parallel arrays with a Josephson junction coupler [2, 9, 13]), the spin-spin interaction strengths $J_{ij}/2\pi$ can reach the 100 MHz scale, two orders of magnitude larger. In this

regime, the circuit becomes highly nonlinear and strongly hybridized with the spin states, and so an additional mode may need to be added for convenient readout [9].

The decoherence rates of the Andreev spins pose a challenge. The existing experimental implementations for Andreev spins rely on the semiconductor InAs, in which confined electronic spins are consistently observed to dephase at the 10 ns scale [6, 8, 37]. The main suspect for this dephasing is the nuclear spin bath of InAs, which should result in a similar scale of decoherence at Kramers' point. Therefore, our proposal can serve as a target for next-generation platforms for Andreev spins, such as in isotopically purifiable germanium [38, 39] and carbon [40]. We remark also that we expect logical quantum information to be protected from charge noise to at least first order at Kramers' point, mitigating a common concern about spin-orbit type qubits [41].

Finally, we speculate on how one might extend to full quantum error correction. One approach is to use a bit flip circuit as a module embedded in a larger quantum error correction circuit; for this, inter-module gates is needed, such as pairwise controlled phase gate between spins hosted in separate modules. This can be done with flux control between inductively coupled weak links as was recently accomplished with Andreev spins [9] or with resonator-mediated couplings as has recently been accomplished with Andreev pair states [42]. Other methods from the superconducting qubit community may also be adapted [26, 27]. As an added remark, it may be possible to expand the set of fault-tolerant quantum gates at Kramers' point through holonomic protocols [43, 44]. We leave the extension to full quantum error correction and fault-tolerant gates to future work.

All data generated and code used in this work are available at: 10.5281/zenodo.14277238.

V. F. acknowledges helpful discussions with Baptiste Royer and Chao-Ming Jian, as well as an early conversation with Christian Andersen on parity readout. We thank Christian Andersen, Baptiste Royer, and Shyam Shankar for input on the manuscript and the concept.

Research was sponsored by the Army Research Office and was accomplished under Grant Number W911NF-22-1-0053. The views and conclusions contained in this document are those of the authors and should not be interpreted as representing the official policies, either expressed or implied, of the Army Research Office or the U.S. Government. The U.S. Government is authorized to reproduce and distribute reprints for Government purposes notwithstanding any copyright notation herein. Research by I.A.D. and A.A. was supported by the Netherlands Organization for Scientific Research (NWO/OCW) as part of the Frontiers of Nanoscience program, a NWO VIDI grant 016.Vidi.189.180. We also thank the Global Quantum Leap sponsored by the National Science Foundation AccelNet program under award number OISE-2020174

for funding an exchange visit by I. A. D.

V. F. conceived the project and coordinated the research. H. L. and B. vH. accomplished initial calculations, and B. vH. wrote down the general analytical approach. I. A. D. and A. A. developed the numerical methods for solving the inductive circuit, and H. L. developed code for calculating the resonator frequency shifts. H. L. and I. A. D. calculated results for the circuits shown in the main text. V. F. wrote the manuscript with input from all authors. The authors declare no competing interests.

Appendix

Solving the circuit

The readout technique of the Andreev spins relies on the spin-dependent inductance of the circuit:

$$E_L = \varphi_0^2 \frac{\partial^2 E_g}{\partial \Phi_{\text{in}}^2} \Big|_{\Phi_{\text{in}}^*}, \quad (4)$$

where E_g is the ground state energy of the circuit, E_L is the inductive energy scale proportional to the inverse inductance, Φ_{in} is the incoming flux through the circuit, and Φ_{in}^* indicates the value of Φ_{in} at the energetic minimum. In this section, we describe how to compute the energies of the 8 spin configurations and their respective inductances.

To solve the circuit, we first write its energy:

$$\mathcal{V} = \sum_{i=1}^3 \left(U_i \left(\frac{\Phi_{B_i}}{\varphi_0} \right) + \frac{\Phi_{T_i}^2}{2L_i} \right) + \frac{\Phi_{M_1}^2}{2L_{12}} + \frac{\Phi_{M_2}^2}{2L_{23}}, \quad (5)$$

where i is the index of each Andreev spin qubit, $U_i(\phi) = E_{J,i} \cos(\phi) + E_{\sigma,i} \sigma_{z,i} \sin(\phi)$ is the Josephson potential of the weak link, and L are the inductances. The branch fluxes Φ_{T_i} , Φ_{B_i} , and Φ_{M_i} label the top, bottom, and middle branches of the circuit, respectively. In terms of the node fluxes, the branch fluxes are:

$$\Phi_{T_1} = \Phi_{\text{in}} - \Phi_{u_1} - \Phi_{e_1}, \quad \Phi_{B_1} = \Phi_{\text{in}} - \Phi_{d_1}, \quad (6a)$$

$$\Phi_{T_2} = \Phi_{u_1} - \Phi_{u_2} - \Phi_{e_2}, \quad \Phi_{B_2} = \Phi_{d_1} - \Phi_{d_2}, \quad (6b)$$

$$\Phi_{T_3} = \Phi_{u_2} - \Phi_{e_3}, \quad \Phi_{B_3} = \Phi_{d_2}, \quad (6c)$$

$$\Phi_{M_1} = \Phi_{u_1} - \Phi_{d_1}, \quad \Phi_{M_2} = \Phi_{u_2} - \Phi_{d_2}, \quad (6d)$$

where Φ_{in} is the input flux to the circuit, Φ_{u_i} and Φ_{d_i} are the node fluxes of the up and down branches' nodes, and Φ_{e_i} are the external fluxes threaded through each circuit loop. Replacing the node fluxes into Eq. (5), rescaling the node fluxes into phase variables, $\phi_i = \Phi_i/\varphi_0$, and substituting the Josephson potential gives:

$$\begin{aligned} \mathcal{V} = & -\sqrt{E_{J_1}^2 + E_{\sigma_1}^2} \cos(\phi_{\text{in}} - \phi_{d_1} - \gamma_1 \sigma_z^{(1)}) \\ & -\sqrt{E_{J_2}^2 + E_{\sigma_2}^2} \cos(\phi_{d_1} - \phi_{d_2} - \gamma_2 \sigma_z^{(2)}) \\ & -\sqrt{E_{J_3}^2 + E_{\sigma_3}^2} \cos(\phi_{d_2} - \gamma_3 \sigma_z^{(3)}) \\ & + \frac{1}{2} E_{L_1} (\phi_{\text{in}} - \phi_{u_1} - \phi_{e_1})^2 \\ & + \frac{1}{2} E_{L_2} (\phi_{u_1} - \phi_{u_2} - \phi_{e_2})^2 \\ & + \frac{1}{2} E_{L_3} (\phi_{u_2} - \phi_{e_3})^2 \\ & + \frac{1}{2} E_{L_{12}} (\phi_{u_1} - \phi_{d_1})^2 \\ & + \frac{1}{2} E_{L_{23}} (\phi_{u_2} - \phi_{d_2})^2. \end{aligned} \quad (7)$$

To compute the inductance of the circuit using Eq. (4), we need to find the energies of the eight spin configurations. Because the energy of the circuit does not depend

on dynamical variables, we find the ground state by minimizing the potential energy for each spin configuration:

$$\frac{\partial \mathcal{V}}{\partial \phi_{u_1}} = \frac{\partial \mathcal{V}}{\partial \phi_{u_2}} = \frac{\partial \mathcal{V}}{\partial \phi_{d_1}} = \frac{\partial \mathcal{V}}{\partial \phi_{d_2}} = 0. \quad (8)$$

This gives a set of four nonlinear coupled equations that determine the values of the internal nodes phase variables ϕ_{u_1} , ϕ_{u_2} , ϕ_{d_1} , ϕ_{d_2} as a function of the external variables ϕ_{in} , ϕ_{e_1} , ϕ_{e_2} , ϕ_{e_3} . A naive approach to solve this system of equations is to solve Eq. (8) numerically using a minimizer for a given set of external phases ϕ_{in} and ϕ_{e_i} , and then compute the second numerical derivative of the energy with respect to the input flux to obtain the inductance. This approach is prone to numerical errors associated with multi-dimensional minimization and numerical differentiation.

We avoid numerical errors by computing an exact solution to Eq. (8) using analytical differentiation. First, we compute the gradient of the potential energy with respect to the internal nodes phase variables and incoming phase using the automatic differentiation library JAX [45]. This gives the system of equations in Eq. (8) with an additional equation for the incoming phase. Second, we solve the five nonlinear coupled equations using a root-finding algorithm [46], and find ϕ_{in}^* , $\phi_{u_1}^*$, $\phi_{u_2}^*$, $\phi_{d_1}^*$, and $\phi_{d_2}^*$ that minimize \mathcal{V} . Finally, we compute the inductive energy E_L as the Schur complement of the Hessian of the potential energy \mathcal{V} , $(\phi_{\text{in}}^*, \phi_{u_1}^*, \phi_{u_2}^*, \phi_{d_1}^*, \phi_{d_2}^*)$. This procedure successfully computes the spin-dependent energy and inductance of the circuit without numerical derivatives or numerical minimization. The procedure is also straightforwardly extensible to additional spins and inductors.

To obtain the dispersive shift, we simulate the Andreev circuit as a termination of a transmission line resonator. The resonance frequency is given by the smallest solution for ω_r in

$$\cot\left(\frac{\omega_r l}{v_{\text{eff}}}\right) = -\frac{iZ_L}{Z_c}, \quad (9)$$

where Z_c is the characteristic impedance, l is the length of the transmission line segment, v_{eff} is the light velocity in the transmission line, and $Z_L = 2i\omega_r\varphi_0^2/E_L$ the impedance of the Andreev circuit obtained from Eq. (4).

We obtain the dispersive shift contribution χ_{ij} and the inter-spin coupling energy J_{ij} from the resonator frequency and ground state energies. We first assume a general form:

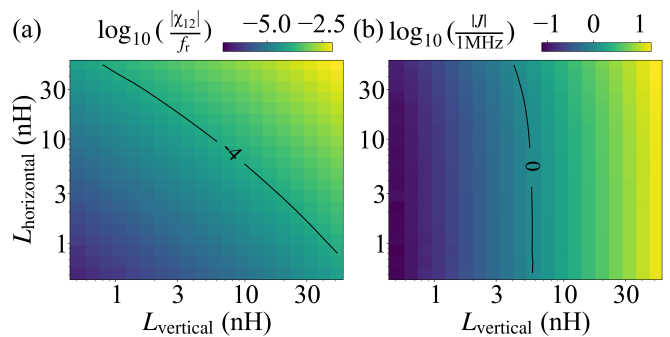


FIG. 3. (a) Dispersive shift χ_{12} and (b) inter-spin coupling J_{12} at Kramers' point. Parameter used in the simulation: $E_{\sigma_1}/h = 0.4$ GHz, $E_{\sigma_2}/h = 0.3$ GHz, $E_{\sigma_3}/h = 0.2$ GHz; $E_{J_1}/h = E_{J_2}/h = E_{J_3}/h = 0.4$ GHz. $L_{\text{vertical}} = L_{12} = L_{23}$ and $L_{\text{vertical}} = L_1 = L_2 = L_3$. For this configuration J_{23} and χ_{23} are of similar scale, while J_{13} and χ_{13} are much smaller.

$$H = J_0 + \sum_{h=1} J_h \sigma_{h,z} + \sum_{h \neq j} J_{hj} \sigma_{h,z} \sigma_{j,z} + J_{123} \sigma_{1,z} \sigma_{2,z} \sigma_{3,z}, \quad (10)$$

$$H_r = \hbar \hat{a}^\dagger \hat{a} \left(\omega_{r,0} + \sum_{h=1} \chi_h \sigma_{h,z} + \sum_{h \neq j} \chi_{hj} \sigma_{h,z} \sigma_{j,z} + \chi_{123} \sigma_{1,z} \sigma_{2,z} \sigma_{3,z} \right). \quad (11)$$

With simulated data from all eight spin configurations, for $Z_c = 50 \Omega$, $v_{\text{eff}} = 0.39c$ (c is the free space speed of light), and varying $l \in [0.1, 3.3]$ mm to fix $\omega_{r,0} = 9$ GHz. We then extract each coefficient in Eqs. (10) and (11). We found that the odd-order terms indeed vanish at Kramers' point, bringing the Hamiltonian to the forms of Eq. (2) and Eq. (3). As an example calculation, Fig. 3 displays J_{12} and χ_{12} as a function of the vertical and horizontal inductances (the inductors of the same orientation are uniform). It shows that the magnitude of the dispersive shift has strong dependence on both vertical and horizontal inductors, while the inter-spin coupling energy depends more on the vertical inductor.

EDSR drive

As pointed out by Padurariu and Nazarov, phase-biased Andreev spins can be driven by a finite-frequency drive on the gate [2]. This is because the spin-orbit polarization pseudovector can depend on the gate voltage. Taking the case a single Andreev spin, they described the following drive Hamiltonian:

$$H(t) = [\vec{\epsilon}_{SO} + \delta \vec{\epsilon}_{SO} \cdot \vec{\sigma} \cos(\omega t)] \sin(\varphi), \quad (12)$$

where $\vec{\epsilon}_{SO}$ is the unperturbed spin-orbit vector, $\delta \vec{\epsilon}_{SO}$ is the modulation of that vector due to the gate with the

condition $|\delta\vec{e}_{SO}| \ll |\vec{e}_{SO}|$, and $\vec{\sigma}$ is the unperturbed Pauli matrix vector. Here we take a simplifying assumption that $\vec{e}_{SO} \propto \hat{z}$ and $\delta\vec{e}_{SO} \propto \hat{x}$, providing

$$H(t) = [E_{\sigma}\sigma_z + M\sigma_x \cos(\omega t)] \sin(\hat{\varphi}) . \quad (13)$$

For the single spin, shunted by an inductance, Kramers' point is at $\langle\hat{\varphi}\rangle = 0$, so that the EDSR drive cannot induce the transition. This method for manipulation of ASQs has been experimentally demonstrated [8, 23].

When an additional spin is in the circuit, it induces a spin-dependent phase bias to the other spins. Taking the three-spin circuit of Figure 1, when the weak link energies are much smaller than the inductive energies, we can approximate the average phase across spin j as

$$\langle\hat{\varphi}_j\rangle \approx \sum_k A_{jk}\sigma_{k,z} , \quad (14)$$

where the dimensionless weights A_{jk} depend on the details of the circuit. Assuming weak spin-spin interactions giving $\langle\hat{\varphi}_j\rangle \ll 1$ (and consistent with simulations), we can Taylor expand the interaction (12) and apply the rotating wave approximation for $\hbar\omega = 2S$ to get

$$H_{d,j} = M\sigma_{j,x} \sum_k A_{jk}\sigma_{k,z} . \quad (15)$$

Finally, we remark that the single-spin transition frequency is conditional on the state of the other spins. For the three-spin circuit, each spin is two spin-transition frequencies: one when the other two spins are aligned, and one where the other two spins are anti-aligned. To obtain an unconditional single-spin rotation, the drive must contain two frequency components resonant to the two transitions (with more frequencies for larger arrays). Multi-frequency control has been accomplished in solid state qubit contexts in several other situations [31–34].

- * vf82@cornell.edu
- [1] N. M. Chtchelkatchev and Y. V. Nazarov, *Physical Review Letters* **90**, 226806 (2003).
 - [2] C. Padurariu and Y. V. Nazarov, *Physical Review B* **81**, 144519 (2010).
 - [3] S. Park and A. L. Yeyati, *Physical Review B* **96**, 125416 (2017).
 - [4] L. Tosi, C. Metzger, M. Goffman, C. Urbina, H. Pothier, S. Park, A. L. Yeyati, J. Nygård, and P. Krogstrup, *Physical Review X* **9**, 011010 (2019).
 - [5] M. Hays, V. Fatemi, K. Serniak, D. Bouman, S. Diamond, G. de Lange, P. Krogstrup, J. Nygård, A. Geresdi, and M. H. Devoret, *Nature Physics* **16**, 1103 (2020).
 - [6] M. Hays, V. Fatemi, D. Bouman, J. Cerrillo, S. Diamond, K. Serniak, T. Connolly, P. Krogstrup, J. Nygård, A. L. Yeyati, A. Geresdi, and M. H. Devoret, *Science* **373**, 430 (2021).
 - [7] A. Bargerbos, M. Pita-Vidal, R. Žitko, L. J. Splitthoff, L. Grünhaupt, J. J. Wesdorp, Y. Liu, L. P. Kouwenhoven, R. Aguado, C. K. Andersen, A. Kou, and B. van Heck, *Physical Review Letters* **131**, 097001 (2023).
 - [8] M. Pita-Vidal, A. Bargerbos, R. Žitko, L. J. Splitthoff, L. Grünhaupt, J. J. Wesdorp, Y. Liu, L. P. Kouwenhoven, R. Aguado, B. van Heck, A. Kou, and C. K. Andersen, *Nature Physics* **19**, 1110 (2023).
 - [9] M. Pita-Vidal, J. J. Wesdorp, L. J. Splitthoff, A. Bargerbos, Y. Liu, L. P. Kouwenhoven, and C. K. Andersen, *Nature Physics*, 1 (2024).
 - [10] M. H. Devoret, S. Girvin, and R. Schoelkopf, *Annalen der Physik* **16**, 767 (2007).
 - [11] T. Vakhtel and B. van Heck, *Physical Review B* **107**, 195405 (2023).
 - [12] T. Vakhtel, P. D. Kurilovich, M. Pita-Vidal, A. Bargerbos, V. Fatemi, and B. van Heck, *Physical Review B* **110**, 045404 (2024).
 - [13] M. Pita-Vidal, J. J. Wesdorp, and C. K. Andersen, *arXiv.org* (2024).
 - [14] C. Chamberland, *Physical Review X* **10**, 10.1103/PhysRevX.10.011022 (2020).
 - [15] S. B. Bravyi and A. Y. Kitaev, *Quantum codes on a lattice with boundary* (1998).
 - [16] E. Dennis, A. Kitaev, A. Landahl, and J. Preskill, *Journal of Mathematical Physics* **43**, 4452 (2002).
 - [17] S. Bravyi, A. W. Cross, J. M. Gambetta, D. Maslov, P. Rall, and T. J. Yoder, *Nature* **627**, 778 (2024).
 - [18] W. Lechner, P. Hauke, and P. Zoller, *Science Advances* **1**, e1500838 (2015).
 - [19] E. Bäumer, *PRX Quantum* **5**, 10.1103/PRXQuantum.5.030339 (2024).
 - [20] H. Kramers, *Proc. Amsterdam Acad* **33** (1930).
 - [21] U. Vool and M. Devoret, *International Journal of Circuit Theory and Applications* **45**, 897 (2017).
 - [22] C. Metzger, S. Park, L. Tosi, C. Janvier, A. A. Reynoso, M. F. Goffman, C. Urbina, A. Levy Yeyati, and H. Pothier, *Physical Review Research* **3**, 013036 (2021).
 - [23] H. Lu, D. F. Boffill, Z. Sun, T. Kane, J. Nygård, M. Kjaergaard, and V. Fatemi, In preparation..
 - [24] M. Rymarz and D. P. DiVincenzo, *Physical Review X* **13**, 021017 (2023).
 - [25] V. Fatemi, P. Kurilovich, M. Hays, D. Bouman, T. Connolly, S. Diamond, N. Frattini, V. Kurilovich, P. Krogstrup, J. Nygård, A. Geresdi, L. Glazman, and M. Devoret, *Physical Review Letters* **129**, 227701 (2022).
 - [26] A. Blais, A. L. Grimsmo, S. M. Girvin, and A. Wallraff, *Reviews of Modern Physics* **93**, 025005 (2021).
 - [27] M. Kjaergaard, M. E. Schwartz, J. Braumüller, P. Krantz, J. I.-J. Wang, S. Gustavsson, and W. D. Oliver, *Annual Review of Condensed Matter Physics* **11**, 369 (2020).
 - [28] Y. Liu, S. Shankar, N. Ofek, M. Hatridge, A. Narla, K. Sliwa, L. Frunzio, R. Schoelkopf, and M. Devoret, *Physical Review X* **6**, 011022 (2016).
 - [29] C. K. Andersen, A. Remm, S. Lazar, S. Krinner, J. Heinesoo, J.-C. Besse, M. Gabureac, A. Wallraff, and C. Eichler, *npj Quantum Information* **5**, 1 (2019).
 - [30] W. P. Livingston, M. S. Blok, E. Flurin, J. Dressel, A. N. Jordan, and I. Siddiqi, *Nature Communications* **13**, 2307 (2022).
 - [31] M. Neeley, M. Ansmann, R. C. Bialczak, M. Hofheinz, E. Lucero, A. D. O'Connell, D. Sank, H. Wang, J. Wenner, A. N. Cleland, M. R. Geller, and J. M. Martinis, *Science* **325**, 722 (2009).
 - [32] E. Champion, Z. Wang, R. Parker, and M. Blok, *Multi-frequency control and measurement of a spin-7/2 system encoded in a transmon qubit* (2024).
 - [33] X. Yu, B. Wilhelm, D. Holmes, A. Vaartjes, D. Schwiabacher, M. Nurizzo, A. Kringhøj, M. R. v. Blankenstein, A. M. Jakob, P. Gupta, F. E. Hudson, K. M. Itoh, R. J. Murray, R. Blume-Kohout, T. D. Ladd, A. S. Dzurak, B. C. Sanders, D. N. Jamieson, and A. Morello, *Creation and manipulation of Schrödinger cat states of a nuclear spin qubit in silicon* (2024).
 - [34] S. Roy, A. Senanian, C. S. Wang, O. C. Wetherbee, L. Zhang, B. Cole, C. P. Larson, E. Yelton, K. Arora, P. L. McMahon, B. L. T. Plourde, B. Royer, and V. Fatemi, *Synthetic high angular momentum spin dynamics in a microwave oscillator* (2024).
 - [35] N. Samkharadze, A. Bruno, P. Scarlino, G. Zheng, D. DiVincenzo, L. DiCarlo, and L. Vandersypen, *Physical Review Applied* **5**, 044004 (2016).
 - [36] M. Pita-Vidal, *Physical Review Applied* **14**, 10.1103/PhysRevApplied.14.064038 (2020).
 - [37] S. Nadj-Perge, S. M. Frolov, E. P. a. M. Bakkers, and L. P. Kouwenhoven, *Nature* **468**, 1084 (2010).
 - [38] G. Scappucci, C. Kloeffel, F. A. Zwanenburg, D. Loss, M. Myronov, J.-J. Zhang, S. De Franceschi, G. Katsaros, and M. Veldhorst, *Nature Reviews Materials* **6**, 926 (2021).
 - [39] L. Lakić, W. I. L. Lawrie, D. van Driel, L. E. A. Stehouwer, M. Veldhorst, G. Scappucci, F. Kuemmeth, and A. Chatterjee, <http://arxiv.org/abs/2405.02013> (2024).
 - [40] S. Park, W. Lee, S. Jang, Y.-B. Choi, J. Park, W. Jung, K. Watanabe, T. Taniguchi, G. Y. Cho, and G.-H. Lee, *Nature* **603**, 421 (2022).
 - [41] P. San-Jose, G. Schön, A. Shnirman, and G. Zarand, *Physica E: Low-dimensional Systems and Nanostructures* **40**, 76 (2007).
 - [42] L. Y. Cheung, R. Haller, A. Kononov, C. Ciaccia, J. H. Ungerer, T. Kanne, J. Nygård, P. Winkel, T. Reisinger, I. M. Pop, A. Baumgartner, and C. Schönenberger, *Photon-mediated long range coupling of two Andreev level qubits* (2023).
 - [43] P. Zanardi and M. Rasetti, *Physics Letters A* **264**, 94 (1999).
 - [44] V. N. Golovach, M. Borhani, and D. Loss, *Physical Review A* **81**, 022315 (2010).

- [45] J. Bradbury, R. Frostig, P. Hawkins, M. J. Johnson, C. Leary, D. Maclaurin, G. Necula, A. Paszke, J. VanderPlas, S. Wanderman-Milne, and Q. Zhang, [JAX: composable transformations of Python+NumPy programs](#) (2018).
- [46] P. Virtanen, R. Gommers, T. E. Oliphant, M. Haberland, T. Reddy, D. Cournapeau, E. Burovski, P. Peterson, W. Weckesser, J. Bright, S. J. van der Walt, M. Brett, J. Wilson, K. J. Millman, N. Mayorov, A. R. J. Nelson, E. Jones, R. Kern, E. Larson, C. J. Carey, Í. Polat, Y. Feng, E. W. Moore, J. VanderPlas, D. Laxalde, J. Perktold, R. Cimrman, I. Henriksen, E. A. Quintero, C. R. Harris, A. M. Archibald, A. H. Ribeiro, F. Pedregosa, P. van Mulbregt, and SciPy 1.0 Contributors, [Nature Methods](#) **17**, 261 (2020).